Magnetism and microstructure in epitaxial $TbFe_2$ (111) thin films

M. Huth* and C. P. Flynn
Department of Physics and Materials Research Laboratory, University of Illinois at Urbana-Champaign, 1110 West Green Street, Urbana, Illinois 61801
(Received 29 April 1998)

We report the epitaxial growth of the highly magnetostrictive Laves phase compound $TbFe_2$, oriented (111) on Mo (110) templates by means of molecular beam epitaxy. The film structure was investigated and related to the magnetic properties. Reflection high-energy electron diffraction showed the growth mode to be Stranski-Krastanov. Pronounced roughening was observed to follow strain relaxation, resulting in a film with deep grooves between islands. Differences of thermal expansion between the sapphire $(11\bar{2}0)$ substrates and the magnetic epilayers place the films under tensile strain at room temperature and below. The magnetic properties of the films are analyzed as the magnetic response of single-domain particles subject to an anisotropic biaxial tensile strain. Dipolar domain coupling and in-plane strain anisotropy caused by the magnetostrictive distortion of domains are discussed for their relevance in explaining the anomalous magnetic hysteresis observed in these $TbFe_2$ thin films. [S0163-1829(98)00741-3]

I. INTRODUCTION

The cubic RFe_2 (R represents rare earth) Laves-phase compounds with $C15$ structure are known for their pronounced magnetic anisotropy and extremely large magnetoelastic constants. These are mainly determined by single-ion effects exerted by the R component. The most thoroughly studied and best understood example of this series of intermetallic compounds is $Tb_{0.3}Dy_{0.7}Fe_2$, also known as Terfenol-D. In Terfenol-D the magnetic anisotropy is greatly reduced compared to the terminal compounds $TbFe_2$ and $DyFe_2$. This happens because in $TbFe_2$ the axes of easy magnetization point towards the $\{111\}$ directions whereas in $DyFe_2$ these axes are aligned along $\{100\}$.[1] Despite the reduced magnetic anisotropy in Terfenol-D a large magnetostriction along the $\{111\}$ directions is preserved. The magnetic properties of the bulk material are now well understood because of the resulting technological importance of Terfenol-D single crystals. More generally, the technical problem of tailoring desired properties is resolved by designing the energetics of the alternative orientations of the moments to create the desired field and temperature dependence. The present research bears on this same problem for the case of materials grown as thin epitaxial films by molecular-beam epitaxy.

Epitaxial films of the RFe_2 series provide a separate challenge. Only very recently it was shown that they can be grown with high quality by molecular-beam epitaxy (MBE).[2,3] The nucleation problem was solved using various refractory templates to obtain (110) or (111) growth at choice.[2–8] The magnetic properties of $DyFe_2$ and $ErFe_2$ (110) are now being investigated[6] but those for $TbFe_2$ are not fully understood.[5] This is mainly due to the fact that epitaxial strain and clamping add further complexity to the interplay of various energy contributions that govern key magnetic parameters in single crystals. Strain changes the magnetic properties, as also does the presence of an interface that breaks the translational symmetry of the lattice. Interface effects are less important in thicker films due to their inverse thickness dependence. In contrast, strain can be sustained through a thick film in several ways. For example, magnetic layers can be sandwiched between nonmagnetic layers that have slightly different lattice constants. Epitaxial strain can then be maintained throughout the magnetic layers by repeating the sandwich as a multilayer, provided that the individual layer thicknesses do not exceed the critical value for the onset of strain relaxation by dislocation mechanisms. This has been studied for rare earth and especially Dy c-axis epilayers.[9] Recently these investigations were extended to films grown along the b axis.[10]

In many instances adhesion of the epilayer to the substrate is sufficient to clamp the films, which then follow the elastic response of the substrate to external parameters like temperature. Therefore strains usually develop in cooling from an elevated growth temperature due to the difference between the thermal expansion coefficients of the substrate and epilayer.

Very little is presently known about these mechanisms for intermetallic compounds grown in the form of thin epitaxial films. In $TbFe_2$ (111) in-plane tensile strain results in anomalous magnetic hyteresis behavior that is not yet satisfactorily explained.

In the work presented here two important issues concerning epitaxial $TbFe_2$ (111) thin films grown on high-quality Mo (110) templates are addressed. The structural evolution of the films during growth and the importance of maintaining the correct stoichiometry are both investigated. Furthermore, the relationship of the magnetic properties to the film microstructure is analyzed. By modeling the films as independent single-domain particles, as suggested by the island structure of the films, the principal features of the magnetic response for individual magnetic domains are calculated. Anisotropic in-plane tensile strain and magnetic dipolar coupling between domains are discussed as possible causes for the anomalous magnetic hysteresis observed here in $TbFe_2$ epitaxial films.

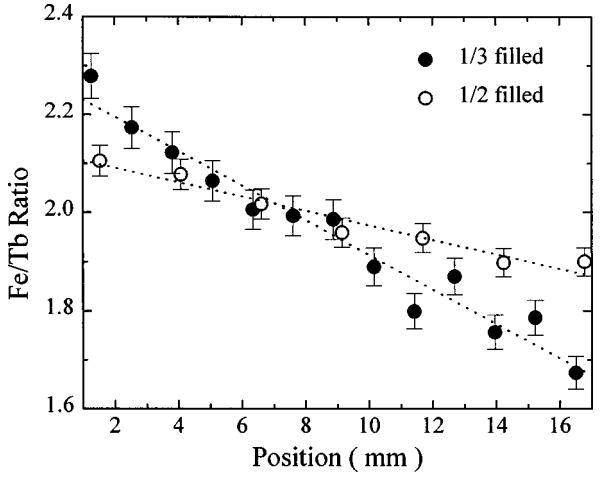

FIG. 1. Compositional gradient in Fe:Tb ratio as determined by Rutherford backscattering for two different filling ratios of the Fe liner as indicated. The horizontal axis represents the position along the long axis of a 17 $\times 4$ mm^2 film.

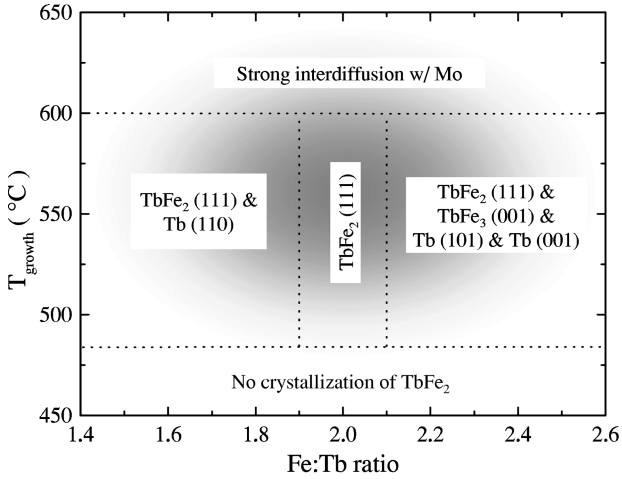

FIG. 2. Phase diagram for the growth of $TbFe_2$ (111) on Mo (110). The dotted lines indicate different growth regimes.

II. EXPERIMENTAL DETAILS

The films were grown in a Perkin Elmer 430 MBE system that maintained a base pressure of 6×10^{-11} Torr. Sapphire substrates in the $(11\bar{2}0)$ *a*-plane orientation were cleaned with basic and organic solvents, and then annealed for 1 h in vacuum at 1000 °C. The Mo (from Johnson Matthey, 99.97% pure) buffer layers were deposited in the (110) orientation by electron-beam evaporation, onto substrates that were held at 750 °C. The growth rate was kept constant at 0.2 Å/s for thicknesses of 400 Å to 500 Å. During buffer-layer growth the pressure increased to about 8×10^{-10} Torr owing to hydrogen released from the source material.

The samples were next cooled to the temperature range 450 °C to 680 °C for deposition of $TbFe_2$ (111). This was accomplished at a growth rate of 0.2 Å/s for film thicknesses of 400 Å to 1500 Å, with a background pressure of 8×10^{-11} Torr. The Fe (Johnson Matthey, 99.9985% pure) and Tb (from the Ames Laboratory, 99.9985% pure) were sublimed from high-temperature effusion cells using high-purity tantalum liners. The Fe to Tb rate ratio was monitored using a quadrupole mass spectrometer. This instrument was calibrated using independent measurements of the film stoichiometry obtained by Rutherford backscattering, the latter employing 2-MeV ^{4}He+ ions directed at an incidence angle of 15° to the film normal. The film structure was investigated *in situ* by reflection high-energy electron diffraction (RHEED) and *ex situ* by x-ray diffraction. The x-ray work employed a two-circle and a four-circle diffractometer using Cu and Mo radiation, respectively. Atomic force microscopy (AFM) was also performed in air on the samples by means of a nanoscope multiprobe microscope. Magnetic properties of the films were investigated in a commercial quantum design superconducting quantum interference device magnetometer.

III. STRUCTURE OF THE FILMS

A. Influence of sample composition

$TbFe_2$ is a peritectic line compound with no volatile components and it is therefore necessary to provide the components in the exact stoichiometric proportions during the deposition process. In order to secure a high degree of structural perfection by avoiding nonstoichiometry, a collimated Fe beam was established using a cylindrical liner with a length-to-diameter ratio of 4:1. The composition of the resulting Tb-Fe alloy varied linearly as a function of position along the sample (see Fig. 1). This was chosen as the long axis of rectangular substrates $15\times4\times0.5$ mm^3 in size. The compositions were determined by Rutherford backscattering. For all further structural studies and magnetic measurements the samples were cut in four to six pieces of typical size 4 $\times 4$ mm^2. Only that part of the sample with the composition Fe:Tb = 2:1 was used for the measurements reported below in order to avoid impurity-phase contributions in the measured properties. When the filling factor of the crucible was changed from 1/3 to 1/2 the composition gradient changed from $\pm15\%$ to $\pm6\%$. This approach allows the investigator to eliminate off-stoichiometry to any required degree.

The growth with graded composition made it possible to establish a phase diagram for the epitaxial growth of $TbFe_2$ (111). This is shown in Fig. 2. The shading in the center of the phase diagram represents the structural quality of the $TbFe_2$ films, with dark areas marking higher structural quality as determined by x-ray diffraction. Impurity phases were observed to form in the off-stoichiometric regions. In particular, for Fe-rich growth $TbFe_3$ is found to grow epitaxially in the (0001) orientation. At elevated growth temperatures, increased interdiffusion occurs at the Mo-$TbFe_2$ interface and this sets an upper limit to the growth temperature for $TbFe_2$ on Mo. All attempts to improve the crystal quality after growth by postannealing at higher temperature in the range of 750 °C to 1000 °C failed for this reason. The interdiffusion of the Mo buffer layer with $TbFe_2$ eventually led to the destruction of the Laves phase.

B. RHEED

The growth of $TbFe_2$ was monitored by RHEED using a 10-kV beam with 5 mA of beam current and an incidence

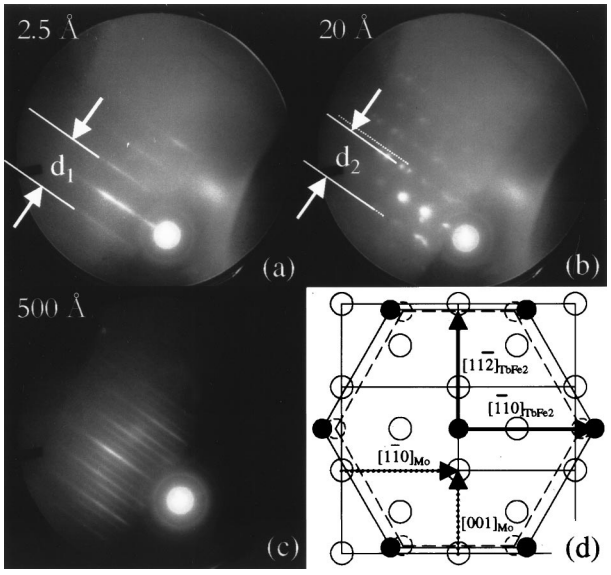

FIG. 3. (a) to (c) RHEED study of the $TbFe_2$ (111) growth on Mo (110) for the film thickness indicated. The beam was aligned along the $[0\bar{1}1]$ direction. (d) Schematic diagram showing the orthorhombic lattice distortion of the $TbFe_2$ (111) surface in the initial pseudomorphic growth stage (dashed lines).

angle $\simeq 0.5°$. The initial growth forms well-defined diffraction streaks. The spacing with the electron beam aligned along $[2\bar{1}1]$ indicates that the films are under $-1.5\% \pm 1.0\%$ compressive strain, whereas with the beam alignment along $[0\bar{1}1]$ a compressive strain of $-12.0\% \pm 1.5\%$ is observed. The orthorhombic distortion of the $TbFe_2$ (111) surface amounts to $+0.5\%$ and -9.1%, respectively, assuming a perfect accommodation of the Mo (110) template at the growth temperature of typically 550 °C. It can then be concluded that the $TbFe_2$ surface is not fully pseudomorphic, most probably due to the large elastic strains involved. The epitaxial relationship and registry of the $TbFe_2$ (111) surface on the Mo (110) surface in the strained and relaxed states is depicted in Fig. 3(d).

As the thickness is increased to the 8- to 10-Å range specular intensity shifts into the diffuse background, indicating a loss of long-range coherence of the film surface. The RHEED image eventually recovers to show spots along the original diffraction streaks. This evidence for three-dimensional scattering is accompanied by a relaxation of the streak spacing towards the lattice constants of unstrained $TbFe_2$ (111). This roughening transition most probably occurs at the onset of dislocation formation. With increasing film thickness the diffraction pattern evolves back to streaks that become well defined at 80 Å. For film thicknesses of 400 Å and more the diffraction pattern reveals that the surface is flat on the length scale of the longitudinal coherence of the electron beam, namely, several thousand Å. The RHEED pattern corresponding to the three growth stages is shown in Fig. 3.

The $TbFe_2$ surface reconstructs through the sequence of 1×1, 3×3, and then 2×2 reconstructions as the temperature is increased from 520 °C to 580 °C. The surface also exhibits (110) facetting as made evident by RHEED and AFM measurements.

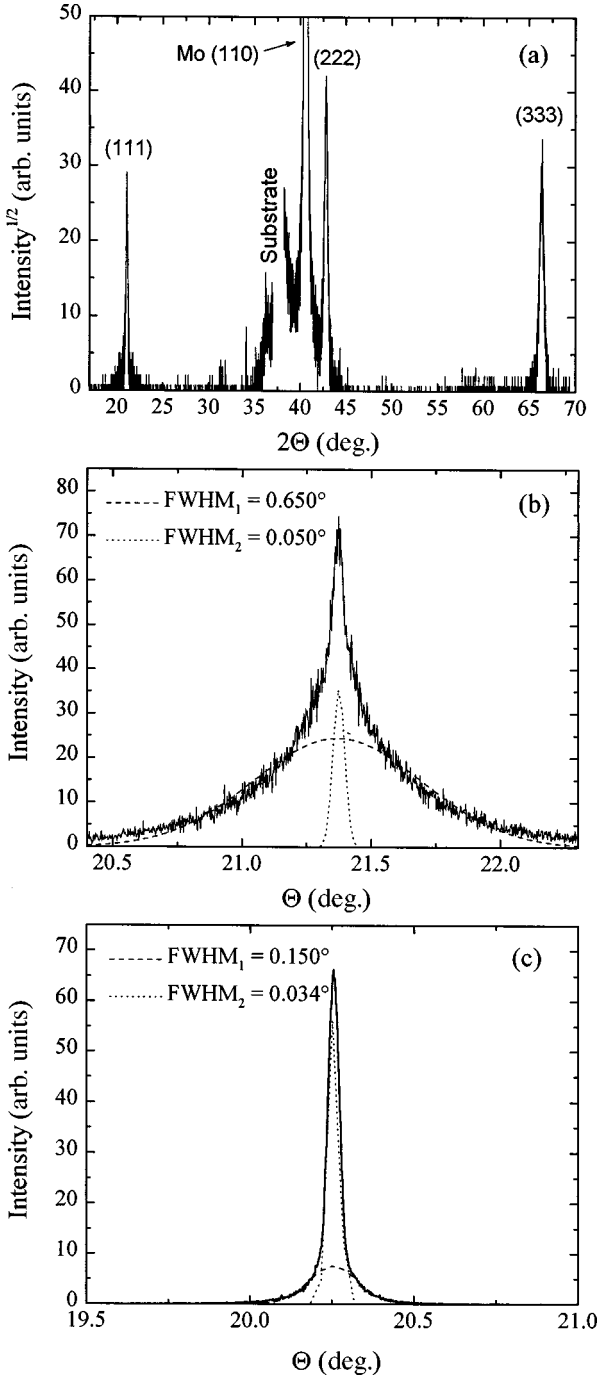

FIG. 4. (a) Longitudinal x-ray scan of $TbFe_2$ (111) on Mo (110). (b) Transversal scan of the $TbFe_2$ (222) reflection, including a two-component analysis of the rocking curves as indicated and (c) transversal scan of the Mo (110) reflection.

C. X-ray diffraction

Prior to its use as a buffer layer, the growth conditions for Mo were optimized. The rocking curves show a two-component line shape, as shown in Fig. 4(c), with variable ratios of spectral weight in the narrow and broad component. The width of the narrow specular component is resolution limited at 0.034° for the (110) reflection. The broad component, whose width is independent of the longitudinal scattering vector, reflects the 0.15° to 0.25° mosaic spread of the crystals. X-ray diffraction shows that the $TbFe_2$ crystal qual-

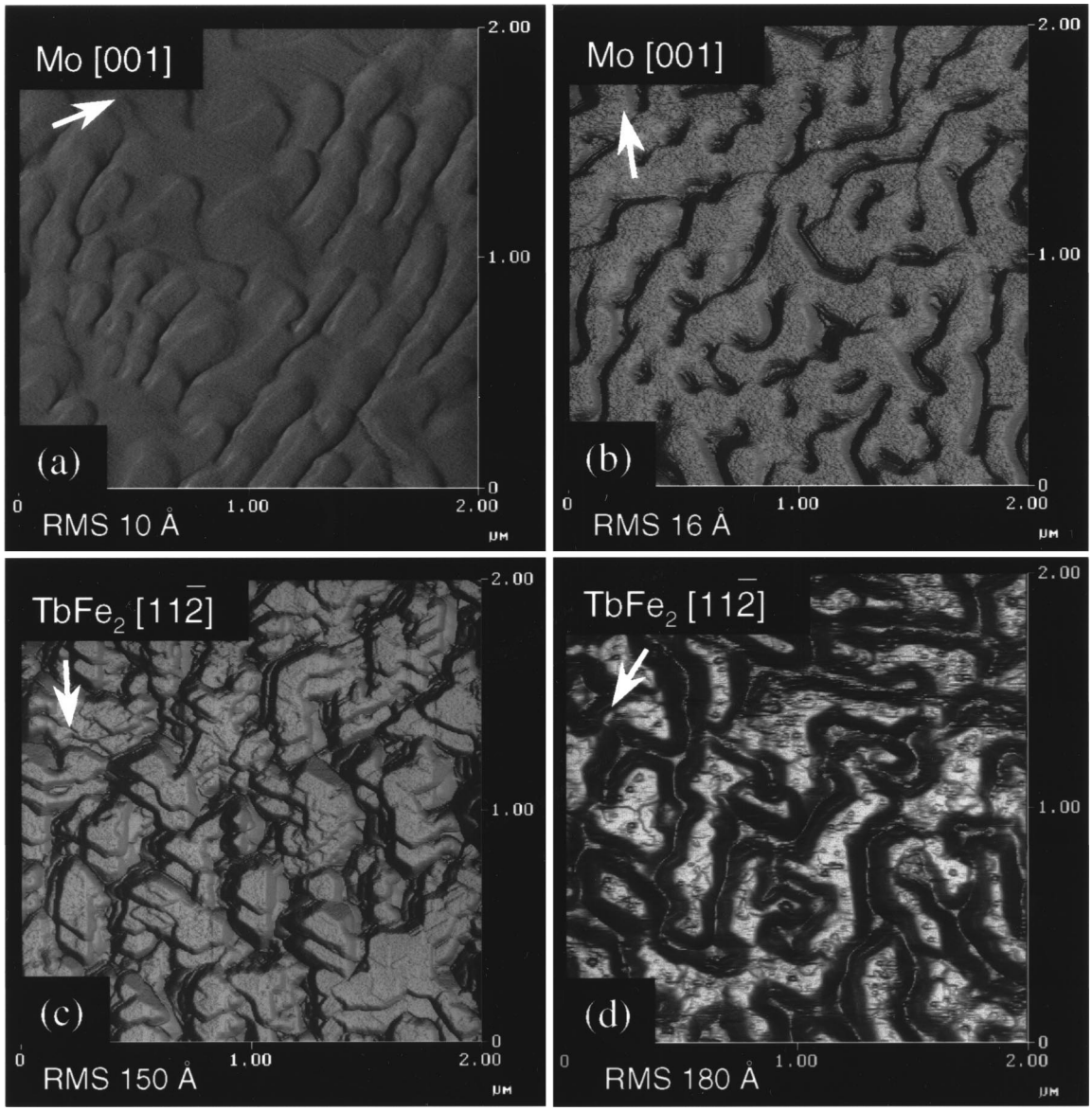

FIG. 5. AFM images of (a) 400 Å of Mo (110) grown on 300 Å of Ta (110) on sapphire $(11\bar{2}0)$; and (b) 400 Å of Mo (110) grown directly on sapphire $(11\bar{2}0)$. The arrow indicates the Mo [001] direction. (c) and (d) show the surface morphologies of $TbFe_2$ (111) grown on these templates. Film thickness is 500 Å in both cases. The arrows indicate the $TbFe_2$ $[11\bar{2}]$ direction.

ity improves with increasing substrate temperature, with crystallization in (111) orientation starting at about 480 °C. A typical Bragg scan is given in Fig. 4(a). The onset of interdiffusion with the Mo buffer layer occurs at temperatures above 580 °C and causes a broadening of the Mo rocking curve and the suppression of the $TbFe_2$ Bragg peaks. In contrast to the results obtained for the $TbFe_2$ (110) growth on Ta (110) (Ref. 3) however, the rocking curves of the (hhh) reflections show no well-defined narrow component. This is shown in Fig. 4(b). A two-component line-shape analysis of the (222) reflection reveals a width of 0.05° for the best samples. This seems to be consistent with the observed roughening that follows the initial pseudomorphic growth. Evidently no long-range height-height correlation is developed among the islands. The vertical displacements of the adatoms caused by dislocation strain fields must result in an increased rms roughness that suppresses the specular reflection in the transverse scans.[11]

ϕ scans of the $TbFe_2$ (022) reflection show sixfold symmetry, which indicates that ABC and ACB stackings occur in equal proportions.

The decrease of the d lattice spacing observed in longitudinal scans shows that the Mo and $TbFe_2$ are under tensile strain. This strain arises from the different thermal expansion coefficients of sapphire and the clamped epilayers. In order to calculate for $TbFe_2$ the in-plane tensile strain that corresponds to the given perpendicular strain of -0.4%, the irreducible elastic constants c^{α} and c^{ϵ} are needed. To the best of our knowledge these have not been measured for $TbFe_2$. The reason for this might be related to the strong magnetic-field dependence of c^{ϵ} and the fact that full magnetic saturation can only be achieved above 10 T due to the large magnetic anisotropy in $TbFe_2$ single crystals. By adopting instead the known elastic constants of Terfenol-D, specifically $c^{\alpha}=271$ GPa and $c^{\epsilon}=97.4$ GPa,[12] the in-plane tensile strain is esti-

mated at 0.5%. c^{ϵ} shows a dependence on magnetic field. The cited value corresponds to the case of magnetic saturation. High-resolution x-ray studies of Wang *et al.*[5] corroborate the calculated 0.5% tensile strain.

D. Atomic force microscopy

AFM reveals that the morphology of $TbFe_2$ depends strongly on the microstructure of the underlying template. Figure 5 shows the morphologies of Mo buffer layers grown on Ta (110) and grown directly on sapphire $(11\bar{2}0)$. The different microstructures of $TbFe_2$ films grown on these templates are also shown in Fig. 5, and show features in common with the underlying Mo.

The percolation network in which Mo grows on sapphire is reproduced in the magnetic layer. When the magnetic layer is grown on the much smoother Mo/Ta template, however, the structure is dominated by largely isolated islands that reflect the symmetry of the $TbFe_2$ (111) surface. In both cases the grooving between $TbFe_2$ islands is pronounced reaching as deep as 60% of the nominal film thickness. The microstructure shows no dependence on the miscut of the sapphire substrates that varied from 1.5° to 0.2°.

The pronounced island structure of $TbFe_2$ films grown on Mo/Ta templates has an important influence on the magnetic hysteresis, as will be evident in the following section.

IV. MAGNETIC PROPERTIES

The axis of easy magnetization was found to be in the plane of the films independent of thickness in the range from 400 Å to 1500 Å. An in-plane easy axis is of course favored due to the shape anisotropy. It is favored also by the 0.5% tensile strain developed in the samples as they cool from the growth temperature to 300 K and below. This strain lowers the free energy for those magnetic domains whose moments are aligned close to {111} crystal axes that lie at a 19° angle to the film plane.

A common feature observed for all samples is a pronounced drop of the magnetization close to or at zero applied field. This occurs in magnetic hysteresis loops measured at various temperatures between 300 K and 5 K. Figure 6 gives results for two 500-Å-thick $TbFe_2$ films whose AFM images are shown in Fig. 5.

Wang *et al.*[5] inferred for sputtered $TbFe_2$ on Mo that this drop in the magnetization is caused by the formation of a magnetic alloy layer in the interfacial region. They studied the dependence of the saturation magnetization on film thickness and found the thickness of the soft magnetic alloy at the interface to be 100 Å.

Hysteresis measurements in the present work do not support their conclusion. A 100-Å-thick alloy region can be responsible for the pronounced magnetization drop for samples as thick as 1500 Å only if the effective saturated moment of the alloy surpasses the saturated moment of $TbFe_2$ by at least an order of magnitude. Furthermore, the saturation magnetization observed in the hysteresis loops taken at room temperature corresponds well to the expected 800 kA/m known for $TbFe_2$ single crystals. Finally, over an extended region of applied field after field reversal the magnetization remains close to zero, as can be seen in Fig. 6. In what follows we propose an alternative mechanism for magnetization reversal that provides a satisfactory account of the observed behavior.

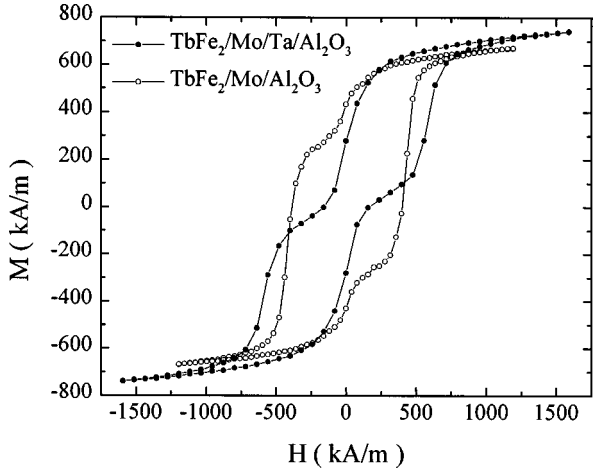

FIG. 6. Magnetic hysteresis loops for two samples with different morphology shown in Fig. 5. The field was aligned parallel to the $TbFe_2$ $[1\bar{1}0]$ direction.

A. Analysis of hysteresis

To begin with, we assume individual magnetic domains that are not coupled. Then the easy axis in zero field must be aligned perpendicular to the field direction, in order to account for the observed drop in magnetization close to zero field. An in-plane strain anisotropy can single out one easy axis of magnetization due to the strong magnetoelastic coupling. In order to estimate the influence of pure one-domain effects on the magnetic hysteresis, a computer program was developed to permit calculation of the hysteresis for a single-domain particle with cubic anisotropy, subject to a biaxial tensile strain in the (111) plane. The results of this calculation represent a necessary prerequisite to understanding the magnetization process, and can later be augmented by consideration of domain coupling effects.

The calculation is based on the energy landscape for a single domain magnetic particle whose moment is rotated with respect to the cubic crystal axes $x=[100]$, $y=[010]$, and $z=[001]$ (the extended Stoner-Wohlfarth model[13]). The orientation of the component magnetizations M_i are specified by polar and azimuthal angles θ and ϕ. Relevant contributions to the energy come from the magnetic anisotropy energy $E_a(\theta,\phi)$, the magnetoelastic energy $E_{me}(\theta,\phi,\{\eta^{\alpha j}\})$, the Zeeman energy $E_z(\theta,\phi,\{H_i\})$, and the demagnetization energy $E_d(\theta,\phi,\{N_{ij}\})$.[14] They may be written

$$E=E_a(\theta,\phi)+E_{me}(\theta,\phi,\{\eta^{\alpha j}\})+E_z(\theta,\phi,\{H_i\}) + E_d(\theta,\phi,\{N_{ij}\}), \quad (1)$$

$$E_a(\theta,\phi)=K_1(a_1^2a_2^2+a_2^2a_3^2+a_1^2a_3^2)+K_2a_1^2a_2^2a_3^2, \quad (2)$$

$$E_{me}(\theta,\phi,\{\eta^{\alpha j}\}) = -\tfrac{3}{2}c^{\gamma}\lambda^{100}\{\tfrac{2}{3}[a_3^2-\tfrac{1}{2}(a_1^2+a_2^2)]\eta^{\gamma 1} + \tfrac{1}{2}(a_1^2-a_2^2)\eta^{\gamma 2}\} - \frac{3}{\sqrt{2}}c^{\epsilon}\lambda^{111} \times (a_1a_2\eta^{\epsilon 1}+a_2a_3\eta^{\epsilon 2}+a_3a_1\eta^{\epsilon 3}), \quad (3)$$

$$E_z(\theta,\phi,\{H_i\}) = -\mu_0\sum_{i=1}^{3} M_iH_i, \quad (4)$$

$$E_d(\theta,\phi,\{N_{ij}\}) = \frac{1}{2}\mu_0\sum_{i,j=1}^{3} M_iN_{ij}M_j. \quad (5)$$

Here the anisotropy constants are K_1 and K_2, the Lagrangian strain variables are $\{\eta^{\alpha j}\}$, the irreducible elastic constants are c^{γ} and c^{ϵ}, the magnetostriction coefficients are λ^{100} and λ^{111} along the [100] and [111] directions, respectively, the components of the demagnetization tensor are N_{ij}, and the applied field is (H_1,H_2,H_3). The a_i are direction cosines with respect to the cube axes.

In order to simulate a typical hysteresis cycle we start with the system in the global energy minimum at zero applied field. This defines the initial direction of the domain moment. The field is then increased to its maximum value, followed by one complete hysteresis cycle. During any field change the magnetization direction is determined by keeping the system adiabatically in a local energy minimum that remains accessible by rotating the moment but without increasing the energy. Thermal excitations into neighboring energy minima that would correspond to thermally induced coherent domain rotation are not taken into account in the present approximation. Since $TbFe_2$ has a high Curie temperature of 698 K,[12] this approach may be adequate even at room temperature.

In Fig. 7(a) results are presented on the basis of the parameters as given in Table I. The Langrangian strain tensors are calulated from x-ray results using the elastic constants of bulk Terfenol-D.

First, an isotropic biaxial strain is assumed based on the material parameters of bulk $TbFe_2$. The resulting hysteresis loop, given by the dashed line in Fig. 7(a), shows a significantly larger coercive field than that observed experimentally and lacks a magnetization drop close to zero field. In order to improve the correspondence between the calculation and measured hysteresis loops K_1 is slightly reduced next [dash-dotted line in Fig. 7(a)]. The easy axes of magnetization are now essentially collinear with the in-plane {112} directions, pointing about 10° out of the plane toward the closest [111] direction.

A magnetization drop that takes place close to zero applied field is reproduced once the magnetoelastic energy contribution $E_{me}(\theta,\phi,\{\eta^{\alpha j}\})$ is allowed to break the sixfold symmetry of the anisotropy energy in the (111) plane, by introducing an anisotropic biaxial strain. Since the easy axis of magnetization under isotropic strain is close to the {112} directions a small elongation along the $[11\bar{2}]$ axis is selected. The result shown as the solid line in Fig. 7(a) predicts a hysteresis loop that is in good agreement with the experimental data. In field reversal close to zero applied field the magnetization discontinously changes its orientation from close to the field direction along $[1\bar{1}0]$ to the easy axis essentially collinear with the $[11\bar{2}]$ direction. The projection of the moment direction in the film plane as it varies during the hysteresis cycle is shown in Fig. 7(b).

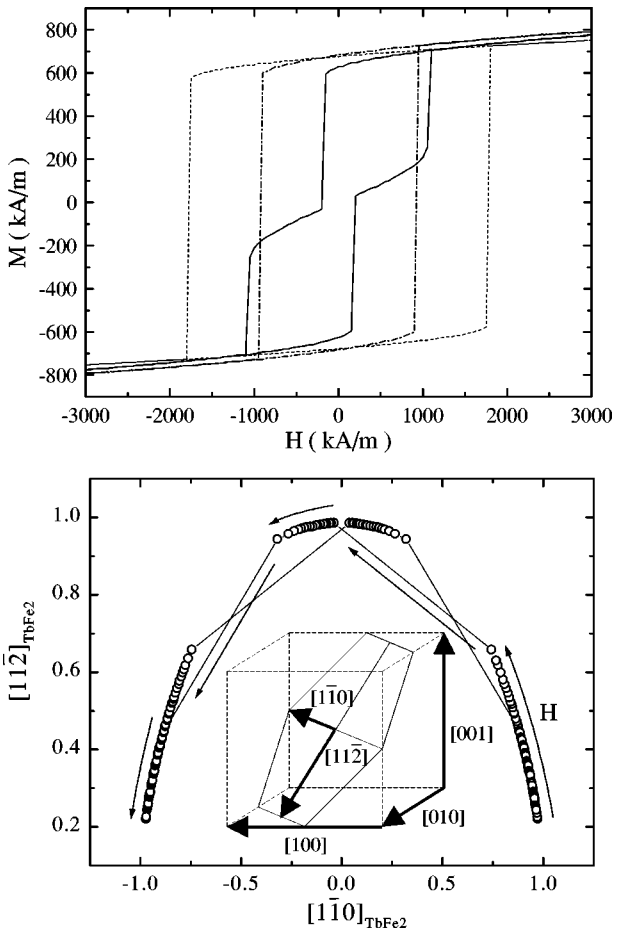

FIG. 7. Results of hysteresis calculation based on the parameters given in Table I (see text for details). Upper figure: The dashed and dash-dotted line assume isotropic tensile strain in the (111) plane for two different values of the anisotropy constants (parameter sets 1 and 2 in Table I). The solid line is obtained when a biaxial strain anisotropy is assumed (parameter set 3 in Table I). Lower figure: The orientation of the moment in the (111) plane for parameter set 3 during a hysteresis loop. The field is aligned parallel to the $TbFe_2$ $[1\bar{1}0]$ direction. The relevant directions are depicted in the inset.

B. Discussion

Domain coupling effects must be taken into account in an improved model because measurements of in-plane hysteresis curves show sixfold symmetry with only weak anisotropy between hysteresis data taken along the {110} and {112} directions. For any given field direction there must then be an appreciable number of domains whose easy axes are aligned perpendicular to the field. This can be accomplished by the following mechanism.

During the cooldown process after growth the sample remains in a demagnetized state below the Curie temperature. In this demagnetized state the individual magnetic domains are subject to biaxial strain since the magnetostrictive energy drives a rhombohedral lattice distortion along easy axes that lie close to the in-plane {112} directions. Minimization of the

TABLE I. Parameters for hysteresis calculation. See text for details.

No.	K_1 (J/m^3)	K_2 (J/m^3)	M_s (A/m)	λ^{111}	λ^{100}	$\eta^{\epsilon 1}=\eta^{\epsilon 2}$	$\eta^{\epsilon 3}$	c^{ϵ} (GPa)
1	-7.6×10^6	0	8×10^5	2.4×10^{-3}	0	-3.0×10^{-3}	-3.0×10^{-3}	97.4
2	-5.0×10^6	0	8×10^5	2.4×10^{-3}	0	-3.0×10^{-3}	-3.0×10^{-3}	97.4
3	-5.0×10^6	0	8×10^5	2.4×10^{-3}	0	-2.3×10^{-3}	-3.3×10^{-3}	97.4

dipolar coupling energy then results in equal populations for all easy axes directions, as dictated by the sixfold structural symmetry in the film plane. On a macroscopic scale the strictions of the individual domains are therefore mutually compensated. The dislocation movements needed to accommodate the microscopic strain fields of any single domain involve one dislocation every 500 lattice sites, assuming about 0.2% magnetostrictve distortion along the easy axes. Given the in-plane lattice constant of 5.2 Å for $TbFe_2$ this results in one dislocation every 260 nm. High-resolution x-ray studies of reflections with an in-plane component of the scattering vector would then show a threefold splitting. Such investigations have not yet been performed on $TbFe_2$ epitaxial films. However, x-ray studies in zero applied field of *c*-axis Dy thin films in the ferromagnetic state show precisely this splitting.[15] With its sixfold symmetry in the basal plane, which is also the plane of easy magnetization, Dy provides a valuable system for comparison.

Suppose that when an external field is applied, the moments begin to align mainly parallel to the field direction. This causes a rotating stress field in the respective domains. The system can respond either with a corresponding rotation of the biaxial strain anisotropy or may instead be clamped, thereby preventing a redistribution of the strains. In the subsequent field reversal of the hysteresis cycle the minimization of the dipolar coupling energy must tend to restore the demagnetized state. When the applied field falls close to zero most domains that point in the original field direction are discontinuously depopulated in favor of symmetry-equivalent easy directions. This discontinuity is supported by the anisotropic strain fields that break the sixfold symmetry each domain would otherwise possess. Only movement and not dislocation creation is necessary to accommodate the local variations of the stress, so the rhombohedral distortion is likely to follow changes of magnetization directions in the domains. However, dislocation creation and motion may in part be thermally activated. It is therefore possible that a crossover could take place from a plastic to a clamped state of the domains as a function of temperature. High-resolution x-ray studies in magnetic fields at various temperatures might possibly clarify this unresolved issue.

The magnetization process of (112) single crystals of $TbFe_2$ under tensile strain along the [112] direction shows comparable switching behavior that was investigated in detail by Jiles and Thoelke.[16]

In concluding this section we relate the microstructure of the films to their magnetic structure. The rough surface morphology of the films suggests that the magnetic domains coincide with the individual structural islands. These are coupled by dipolar interactions. Whether islands with typical diameters ranging from 300 nm to 600 nm do in fact form single domains must remain open to investigation by magnetic imaging techniques, such as magnetic force microscopy (MFM). Note that MFM studies of amorphous $TbFe_2$ films grown on Si/SiO_2 with perpendicular easy axis show that stripe domains are formed whose period varies as the square root of the film thickness.[17] Extrapolating these results to 500-Å-thick films suggests domain sizes of 450 nm. In the present case the films are magnetized in plane and the stray field energy is greatly reduced, which would tend to stabilize even larger domains. Recent MFM studies on the (111) surface of $TbFe_2$ single crystals also show domain sizes on the μm length scale.[18]

With regard to possible technical applications we note that, in highly magnetostrictive films, the elastic moduli change under the influence of an applied magnetic field. This can serve as a means for reducing the speed of propagation of surface acoustic waves.[19] Optimal behavior can only be achieved if the axis of easy magnetization of the films can be aligned perpendicular to the film surface. This represents the only direction in which magnetostriction can freely strain the film. Furthermore, the use of a substrate material that allows the direct coupling of the surface acoustic wave in the delay device is advantageous. The use of piezoelectric substrate materials with large thermal expansion coefficients can account for both conditions. In the clamped state the films are put under compressive strain in the cooling process after growth which then can overcome the shape anisotropy. In other work, to be published elsewhere, we have grown epitaxial $TbFe_2$ (111) on $LiNbO_3$ (111) by means of an appropriate selection of buffer layers. The films are under compressive strain which results in a desirable perpendicular magnetization. Details of this work, which is still in progress, will be published in due course.

V. CONCLUSIONS

The structure and magnetic properties of $TbFe_2$ (111) grown on Mo (110) by molecular-beam epitaxy was investigated. Pseudomorphic growth occurs only up to a film thickness of 8 Å to 10 Å followed by strain relaxation that causes an increased layer roughness. The resulting microstructure consists largely of isolated islands. The magnetic hysteresis was modeled using an anisotropic single-domain model of the Stoner-Wohlfarth type. An in-plane biaxial strain anisotropy required by the model may be attributed to the magnetostrictive distortions of individual domains. The magnetoelastic energy then introduces a new easy axis of magnetization near zero applied field. This explains the observed drop in the magnetization close to zero field.

The properties of epitaxially grown $TbFe_2$ reveal an intimate relationship between the magnetism and the microstructure of the films. Further studies are needed to clarify possible mechanisms of in-plane clamping and plastic evolution of magnetostrictive strain fields during the magnetization process. Nevertheless, the results obtained in this work

suggest how to proceed to possible technological applications that are briefly addressed in the text.

ACKNOWLEDGMENTS

The synthesis was supported in part by the U.S. Department of Energy under Award No. DEFG02-96ER45439 and the magnetic measurements by the National Science Foundation Grant No. DMR-9424339. The x-ray studies were performed in the Center for Microanalysis of Materials of the Materials Research Laboratory, and the AFM measurements were performed in the Beckman Institute. One of us (M.H.) thanks the Deutsche Forschungsgemeinschaft for additional support.

*Present address: Institut für Physik, Johannes Gutenberg-Universität, Mainz, Germany. Electronic address: huth@mail.uni-mainz.de

[1] A. E. Clark, in *Handbook of the Physics and Chemistry of Rare Earth*, edited by K. A. Gschneidner and L. Eyring (North-Holland, Amsterdam, 1982), Vol. 2.

[2] V. Oderno, C. Dufour, K. Dumesnil, Ph. Mangin, and G. Marchal, J. Cryst. Growth **165**, 175 (1996).

[3] M. Huth and C. P. Flynn, J. Appl. Phys. **83**, 7261 (1998).

[4] C. T. Wang, R. M. Osgood III, R. L. White, and B. M. Clemens, in *Magnetic Ultrathin Films, Multilayers and Surfaces*, edited by A. Fert, H. Fujimori, G. Guntherodt, B. Heinrich, W. F. Egelhoff, Jr., and E. E. Marinero, MRS Symposia Proceedings, Vol. 384 (Materials Research Society, Pittsburgh, 1995).

[5] C. T. Wang, B. M. Clemens, and R. L. White, IEEE Trans. Magn. **32**, 4752 (1996).

[6] V. Oderno, C. Dufour, K. Dumensnil, Ph. Bauer, Ph. Mangin, G. Marchal, L. Hennet, and G. Patrat, Europhys. Lett. **36**, 713 (1996).

[7] V. Oderno, C. Dufour, K. Dumesnil, Ph. Bauer, Ph. Mangin, and G. Marchal, Phys. Rev. B **54**, R17 375 (1996).

[8] S. Jaren, E. du Trémolet de Lacheisserie, D. Givord, and C. Meyer, J. Magn. Magn. Mater. **165**, 172 (1997).

[9] F. Tsui and C. P. Flynn, Phys. Rev. Lett. **71**, 1462 (1993).

[10] K. A. Ritley and C. P. Flynn, Appl. Phys. Lett. **72**, 170 (1998).

[11] P. F. Miceli, J. Weatherwax, T. Krentsel, and C. J. Palmstrom, Physica B **221**, 230 (1996); P. F. Miceli and C. J. Palmstrom, Phys. Rev. B **51**, 5506 (1995).

[12] A. E. Clark, in *Ferromagnetic Materials*, edited by E. P. Wohlfarth (North-Holland, Amstedam, 1980).

[13] E. C. Stoner and E. P. Wohlfarth, Philos. Trans. R. Soc. London, Ser. A **240**, 599 (1948); E. W. Lee and J. E. L. Bishop, Proc. Phys. Soc. London **89**, 661 (1966).

[14] Etienne du Trémolet de Lacheisserie, *Magnetostriction* (CRC Press, Boca Raton, FL, 1993).

[15] R. S. Beach, A. Matheny, M. B. Salamon, C. P. Flynn, J. A. Borchers, R. W. Erwin, and J. J. Rhyne, J. Appl. Phys. **73**, 6901 (1993).

[16] D.C. Jiles and J. B. Thoelke, J. Magn. Magn. Mater. **134**, 143 (1994).

[17] Q. Su, Y. Zheng, A. Roytburd, and M. Wuttig, Appl. Phys. Lett. **66**, 2424 (1995).

[18] D. G. Lord, A. P. Holden, and P. J. Grundy, J. Appl. Phys. **81**, 5728 (1997).

[19] H. Uchida, M. Wada, K. Koike, H. H. Uchida, V. Koeninger, Y. Matsumura, H. Kaneko, and T. Kurino, J. Alloys Compd. **211/212**, 576 (1994); V. Koeninger, Y. Matsumura, H. H. Uchida, and H. Uchida, *ibid.* **211/212**, 581 (1994).